View metadata, citation and similar papers at core.ac.uk

brought to you by CORE

provided by Springer - Publisher Connector

Article

Chinese Science Bulletin

Progress of Projects Supported by NSFC
Applied Physics

January 2012 Vol.57 No.1: 20–24
doi: 10.1007/s11434-011-4859-3

Evolution of resistive switching polarity in Au/Ar^+ bombarded $SrTi_{0.993}Nb_{0.007}O_3$/In sandwiches

XIE GuanLin[1], WANG YuHang[1], REN TianLing[2], ZHU JiaLin[1], SUN JiaLin[1] & ZHANG LiuWan[1*]

[1] *Laboratory of Advanced Materials, State Key Laboratory of Low-Dimensional Quantum Physics, Department of Physics, Tsinghua University, Beijing 100084, China;*
[2] *Institute of Microelectronics, Tsinghua University, Beijing 100084, China*

Received May 17, 2011; accepted June 20, 2011

We investigated the resistive switching characteristics of Au/Ar^+ bombarded $SrTi_{0.993}Nb_{0.007}O_3$/In sandwiches. The evolution of the resistive switching polarity with sweeping voltage was observed. Our experiments showed that under a macroscopic electrode the homogeneous trapping-detrapping-type conduction and filament-type conduction coexist and compete with each other. For a large sweeping voltage range, the trapping-detrapping-type conduction dominates. However, for a small range the latter dominates. If the bias voltage is too large, the filament conduction could be destroyed. These results will help deepen the understanding of the resistive switching polarity, and will aid in future device design.

bipolar resistance switching, *I-V* curves, switching polarity

Citation: Xie G L, Wang Y H, Ren T L, et al. Evolution of resistive switching polarity in Au/Ar^+ bombarded $SrTi_{0.993}Nb_{0.007}O_3$/In sandwiches. Chin Sci Bull, 2012, 57: 20–24, doi: 10.1007/s11434-011-4859-3

Because of the increasing demand for miniaturization in microelectronics, nonvolatile resistance random access memory (RRAM) based on sandwich unit cells composed of metal/transition metal oxide (TMO)/metal has attracted considerable attention in the past few years [1–6]. The cell resistance can be switched between different levels using an applied voltage. In a bipolar switching system, the low and high resistance states (LRS, HRS) are set and reset by the different polarity of the applied voltage. Two basic switching models have been proposed. One is the filament conduction model [4,6–9], and the other is the homogeneous Schottky-type switching model [5,10,11]. Note that the two switching mechanisms result in different switching polarities. For n-type semiconductors and a voltage sweeping sequence of 0 V→V_+→0 V→ V_-→ 0 (here V_+ and V_- are the maximum positive and negative applied voltages, respectively), the filament conduction model predicts that the resistance will change from a LRS to a HRS for a positive voltage, and vice versa for a negative voltage. Therefore, a "Counter-Figure-8" hysteretic current-voltage (*I-V*) curve is observed. However, the Schottky-type switching model changes the resistance from a HRS to a LRS for a positive bias, and vice versa for a negative bias, resulting in a "Figure-8" hysteretic *I-V* curve. Nb-doped $SrTiO_3$ (NSTO) single crystal is commonly used as a conductive substrate for functional perovskite oxide thin films. Its resistive switching characteristics have been intensively investigated [5,11–13]. To the best of our knowledge, only "Figure-8" *I-V* curves have been reported. Recently, both "Figure-8" and "Counter-Figure-8" *I-V* curves were observed simultaneously in thick defective Sr_2TiO_4 [14] and Fe-doped $SrTiO_3$ (STO) films [15]. However, the dynamic evolution process was not detailed in the reports.

It is widely accepted that after forming process, bipolar resistive switching occurs at the active metal/TMO interface [16,17]. Therefore, we believe that by modifying the active interface we can control the bipolar resistive switching properties. In this work, we modified the NSTO surface via

*Corresponding author (email: lwzhang@tsinghua.edu.cn)

© The Author(s) 2012. This article is published with open access at Springerlink.com

ion bombardment and investigated the resistive switching characteristics of Au/Ar^+ bombarded NSTO/In sandwiches. Both “Figure-8” and “Counter-Figure-8” *I-V* curves as well as an unexpected bias-dependent evolution process were observed.

1 Experimental

Single-crystal NSTO (001) (0.5 mm thick) samples with a doping level of 0.7 wt% were uniformly bombarded with Ar^+ ions in a Gatan 682 Precision Etching Coat System (Pleasanton, CA, USA) for 20 min (sample A) and 40 min (sample B). A beam energy of 4 keV and a current density of 0.5 mA/cm^2 were used. Gold was sputtered on the bombarded surface over an area with a diameter of 0.8 mm to serve as the top electrode. The bottom electrode was prepared by pressing indium on the opposite NSTO surface, which resulted in good ohmic contact [18]. For comparison, test sample C was prepared on an unbombarded single-crystal NSTO with the same electrode configuration by the same fabrication process. The *I-V* curves were measured with two-probe configuration using a Keithley 2400 source meter. The positive bias is defined by the current flowing from the top Au electrode through NSTO to the bottom In electrode. The voltage sweeping sequence was 0 V→V_+→0 V→ V_-→ 0 V. The bias voltage dependent capacitance at 1 kHz was measured using a QuadTech 1730 LCR meter. All measurements were done at room temperature. X-ray photoelectron spectra (XPS) were acquired using a PHI15300/ESCA system. Al Kα radiation (1484.6 eV) was used as the source, and the C 1s peak was used as a reference.

2 Results and discussion

Figure 1 shows the bias-dependent capacitance and Ti 2p core-level XPS of samples A, B and C. After Ar^+ bombardment, the capacitance greatly decreased and was less sensitive to the bias. At zero bias, the capacitance of sample C was 31.6 nF. While the corresponding values for samples A and B were 7.5 nF and 5.2 nF, respectively. Kan et al. [19] reported that after Ar^+ beam bombardment, an amorphous layer with a few nanometers in thickness was formed on the STO surface. Because the capacitance of the amorphous insulating surface layer is in series with that of the depletion region of the underlying bulk NSTO, a large fraction of the built-in potential drops across this amorphous layer. Therefore, the dependence of the total capacitance on the applied bias is small. Longer-time Ar^+ bombardment introduced thicker amorphous layer, which leads to a smaller capacitance (Figure 1(a)). The XPS experiment showed that after Ar^+ bombardment the binding energy of the Ti $2p_{3/2}$ state was reduced from 459.1 eV (sample C) to 458.6 eV (sample A) or 457.9 eV (sample B). Oxygen loss and structural distortion induced via the Ar^+ bombardment may lead to a decrease in the coordination number of oxygen ions around the Ti ions, which may be responsible for the reduction in the binding energy of the Ti $2p_{3/2}$ state. This is in accordance with the previous XPS investigations on undoped STO [20].

The evolution of the *I-V* characteristics of sample B with sweeping voltage is presented in Figure 2. No pre-forming process was performed. For the range ±1 V (Figure 2(a)), all of the *I-V* curves exhibited the “Figure-8” hysteretic characteristic, which is similar to that of sample C. This can be explained by the electron trapping-detrapping effects at the Au/NSTO interface. For the same bias, the current in sample B is six orders of magnitude smaller than that in sample C because of the insulating surface layer after Ar^+ bombardment.

Figure 2(b)–(d) show the first three *I-V* cycle sequences for $|V_+|=|V_-|=2$ V. The switching polarity of Figure 2(b) is the same as that in Figure 2(a), but the hysteresis is larger. For the second voltage cycle (Figure 2(c)), a current jump occurs near −0.8 V, which suggests the initiation of filament-type conduction. Following the current jump is a negative differential resistance (NDR) region which was also observed in La_2CuO_4 [5], $Pr_{0.7}Ca_{0.3}MnO_3$ [10], Fe doped STO [15] and TiO_2 [21]. Both clockwise and anticlockwise

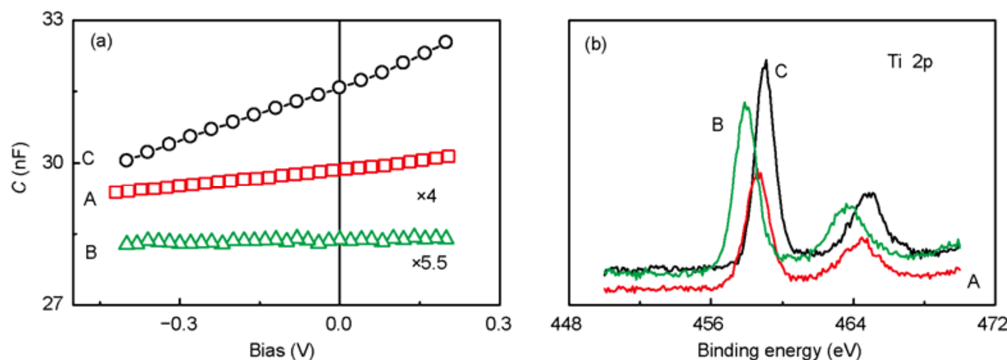

Figure 1 (a) Bias-dependent capacitance and (b) Ti 2p core-level XPS of sample A (red), sample B (green) and sample C (black). To facilitate comparison, the capacitance values for samples A and B in (a) were multiplied by 4 and 5.5, respectively.

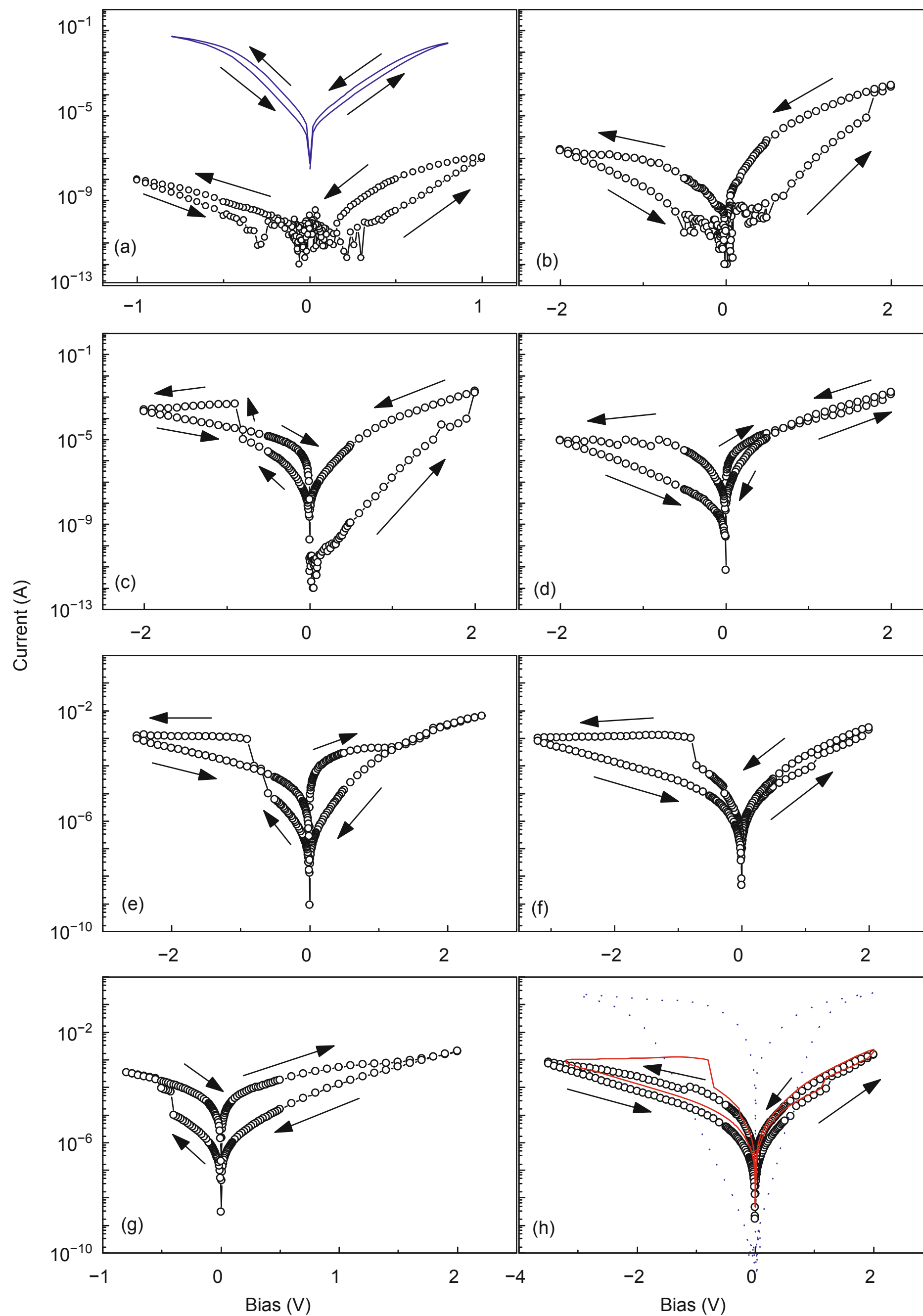

Figure 2 Evolution of the *I-V* characteristics of sample B (black open circles) for the sequent sweeping voltage ranges. (a) (–1 V, 1 V); (b)–(d) (–2 V, 2 V); (e) (–2.5 V, 2.5 V); (f) (–3.2 V, 2 V); (g) (–0.8 V, 2 V) after (e); and (h) (–3.5 V, 2 V). For comparison, *I-V* curves for sample C are also presented in (a) (solid blue line) and (h) (dotted blue line). In (h), the *I-V* curve shown in (f) is re-plotted (solid red line).

hystereses were observed in the negative voltage branch. However, for the third cycle, the two types of hysteresis appear in the positive voltage branch. If we keep cycling the voltage in the range of ±2 V, *I-V* patterns similar to that shown in Figure 2(c) are most likely to occur. However, *I-V* patterns similar to that shown in Figure 2(d) occasionally appear, which indicates that the former is more stable than the latter. The coexistence and unpredictability of the two types of *I-V* hysteresis also imply that there is competition between the filament-type and homogeneous trapping-detrapping-type conduction mechanisms. For cycles in the range of ±2.5 V, the *I-V* curve shown in Figure 2(e) is reproducible. Similar to the pattern shown in Figure 2(c), mixed hysteresis occurs for a negative bias. However, in the positive branch, Figure 2(e) displays the clockwise *I-V* characteristics.

If the swept voltage range is increased to (–3.2 V, 2 V), the obtained *I-V* curve exhibits only “Figure-8”-type hyste-

resis in spite of the current jumping in the negative branch (Figure 2(f)). This indicates that the homogeneous trapping-detrapping conduction mechanism is dominant in this case. After completing a cycle as in Figure 2(e) or (f), we limited the swept range to ($-V_j$, 2 V) (here $-V_j$ is the negative voltage just above which a current jump occurs). The resultant *I-V* curve will have the stable "Counter-Figure-8" resistance switching polarity shown in Figure 2(g). This implies that for the smaller negative bias the filament-type conduction mechanism dominates. However, the larger negative sweeping voltage enhances the homogeneous trapping-detrapping-type conduction.

After we further increase the sweeping voltage range to (−3.5 V, 2 V), the previously observed current jump disappears, and only the small hysteresis with a "Figure-8" type switching polarity is observed (Figure 2(h)). For comparison, the *I-V* curve shown in Figure 2(f) and the curve for sample C for a similar sweeping range are re-plotted in Figure 2(h) with solid red and dotted blue lines, respectively. Note that at the negative bias the current in the HRS of the (−3.5 V, 2 V) cycle (black open circles) is nearly the same as that of the (−3.2 V, 2 V) cycle (solid red line). However, the current in the LRS of the former is much lower than that of the latter. The difference is primarily caused by the filament-type conduction. The currents in both LRSs of sample B are almost two orders of magnitude smaller than that of sample C, which suggests the existence of an insulating surface layer on the bombarded sample B.

Combined with the capacitance and XPS measurements, the measured *I-V* characteristics may be qualitatively explained by the following: Ar^+ bombardment introduced a large quantity of surface states. The trapping and detrapping of electrons in the surface states leads to the "Figure-8" resistance switching polarity shown in Figure 2(a). With an increase in the maximum swept voltage, more electrons become involved in the trapping-detrapping process, which results in a larger *I-V* hysteresis (Figure 2(b)). Dissipated heat increases and was accumulated as the cycle number increases. Thermally-assisted oxygen vacancy migration along the extended defects in the amorphous layer under the strong electric field created by the reverse bias accelerates the formation of conductive filament(s) within the amorphous layer, leading to the current jumping at the negative bias in Figure 2(c). Muenstermann et al. [15] observed that the homogeneous conduction region and the filament conduction region were spatially separated. Both conduction mechanisms coexist and compete. Therefore, both clockwise and anticlockwise *I-V* hysteresis can be observed in one voltage sweep cycle (see Figure 2(c), (d) and (e)). In low swept voltage ranges, the filament-type conduction mechanism dominates. Consequently, "Counter-Figure-8" switching polarity was observed (Figure 2(g)). By contrast, for high swept voltage ranges, the homogeneous trapping-detrapping-type conduction mechanism was greatly enhanced and was dominant. Correspondingly, "Figure-8" resistance switching polarity can be seen in Figure 2(f). With further increase in the swept voltage, the sample is annealed through current-induced self-heating. The defect region in the filament was cured, and the whole sample tended to be homogeneous. Therefore, the current jumping disappeared, and the *I-V* curve exhibited a "Figure-8"-type characteristic (Figure 2(h)).

3 Conclusions

We investigated the swept-voltage-dependent evolution of the resistance switching polarity of Au/Ar^+ bombarded $SrTi_{0.993}Nb_{0.007}O_3$/In heterojunctions. We found that for a small swept voltage range, "Figure-8"-type resistance switching polarity was observed. With an increase in the swept voltage range, a series of mixed resistive switching polarities was observed. For even larger swept voltage ranges, the *I-V* curves return to the "Figure-8"-type hysteresis. Our results can be explained by the coexistence and competition of filament-type and homogeneous trapping-detrapping conduction mechanisms. Our experiments indicate that the resistance switching polarity can be controlled using an external voltage bias, which may aid in future device design.

This work was supported by the National Natural Science Foundation of China (11074142, 11021464), the National Basic Research Program of China (2011CB921904), the Key Project of the Chinese Ministry of Education (309003) and the Tsinghua TNList Cross-discipline Foundation.

1 Liu S Q, Wu N J, Ignatiev A. Electric-pulse-induced reversible resistance change effect in magnetoresistive films. Appl Phys Lett, 2000, 76: 2749–2751

2 Beck A, Bednorz J G, Gerber Ch, et al. Reproducible switching effect in thin oxide films for memory applications. Appl Phys Lett, 2000, 77: 139–141

3 Xia Y, He W, Chen L, et al. Field-induced resistive switching based on space-charge-limited current. Appl Phys Lett, 2007, 90: 022907

4 Waser R, Aono M. Nanoionics-based resistive switching memories. Nat Mater, 2007, 6: 833–840

5 Sawa A. Resistive switching in transition metal oxides. Mater Today, 2008, 11: 28–36

6 Waser R, Dittmann R, Staikov G, et al. Redox-based resistive switching memories—nanoionic mechanisms, prospects, and challenges. Adv Mater, 2009, 21: 2632–2663

7 Szot K, Speier W, Bihlmayer G, et al. Switching the electrical resistance of individual dislocations in single-crystalline $SrTiO_3$. Nat Mater, 2006, 5: 312–320

8 Kim K M, Choi B J, Shin Y C, et al. Anode-interface localized filamentary mechanism in resistive switching of TiO_2 thin films. Appl Phys Lett, 2007, 91: 012907

9 Lian W T, Long S B, Lu H B, et al. Approaches for improving the performance of filament-type resistive switching memory. Chin Sci Bull, 2011, 56: 461–464

10 Sawa A, Fujii T, Kawasaki M, et al. Hysteretic current-voltage characteristics and resistance switching at a rectifying $Ti/Pr_{0.7}Ca_{0.3}MnO_3$ interface. Appl Phys Lett, 2004, 85: 4073–4075

11 Shang D S, Sun J R, Shi L, et al. Electronic transport and colossal electroresistance in $SrTiO_3$: Nb-based Schottky junctions. Appl Phys Lett, 2009, 94: 052105

12 Muenstermann R, Dittmann R, Szot K, et al. Realization of regular arrays of nanoscale resistive switching blocks in thin films of Nb-doped $SrTiO_3$. Appl Phys Lett, 2008, 93: 023110
13 Park C, Seo Y, Jung J, et al. Electrode-dependent electrical properties of metal/Nb-doped $SrTiO_3$ junctions. J Appl Phys, 2008, 103: 054106
14 Shibuya K, Dittmann R, Mi S, et al. Impact of defect distribution on resistive switching characteristics of Sr_2TiO_4 thin films. Adv Mater, 2010, 22: 411–414
15 Muenstermann R, Menke T, Dittmann R, et al. Coexistence of filamentary and homogeneous resistive switching in Fe-doped $SrTiO_3$ thin-film memristive devices. Adv Mater, 2010, 22: 4819–4822
16 Baikalov A, Wang Y Q, Shen B, et al. Field-driven hysteretic and reversible resistive switch at the Ag-$Pr_{0.7}Ca_{0.3}MnO_3$ interface. Appl Phys Lett, 2003, 83: 957–959
17 Fujii T, Kawasaki M, Sawa A, et al. Electrical properties and colossal electroresistance of heteroepitaxial $SrRuO_3/SrTi_{1-x}Nb_xO_3$ ($0.0002 \leqslant x \leqslant 0.02$) Schottky junctions. Phys Rev B, 2007, 75: 165101
18 Cui Y M, Zhang L W, Wang C C, et al. Strain-assisted tunneling current through $TbMnO_3$/Nb-1wt%-doped $SrTiO_3$ p-n junctions. Appl Phys Lett, 2005, 86: 203501
19 Kan D, Terashima T, Kanda R, et al. Blue-light emission at room temperature from Ar^+-irradiated $SrTiO_3$. Nat Mater, 2005, 4: 816–819
20 Henrich V E, Dresselhaus G, Zeiger H J. Surface defects and the electronic structure of $SrTiO_3$ surfaces. Phys Rev B, 1978, 17: 4908–4921
21 Jeong D S, Schroeder H, Breuer U, et al. Characteristic electroforming behavior in Pt/TiO_2/Pt resistive switching cells depending on atmosphere. J Appl Phys, 2008, 104: 123716

Open Access This article is distributed under the terms of the Creative Commons Attribution License which permits any use, distribution, and reproduction in any medium, provided the original author(s) and source are credited.